THE JOURNAL OF PHYSICAL CHEMISTRY C

Article

Cite This: J. Phys. Chem. C 2018, 122, 2113−2121

pubs.acs.org/JPCC

Enhancement of Thermal Energy Transport across the Gold−Graphene Interface Using Nanoscale Defects: A Molecular Dynamics Study

Sadanandam Namsani and Jayant K. Singh*

Department of Chemical Engineering, Indian Institute of Technology Kanpur, Kanpur-2018016, India

Supporting Information

ABSTRACT: Graphene−metal nanocomposites are promising materials to address the heat dissipation problems in nanoscale electronic and computing devices. A low resistance interface between metal and graphene contact is crucial for the development of highly efficient nanodevices. In this direction, we have investigated the thermal conductance (TC) across the gold−graphene interface for various thicknesses of the graphene layer and temperatures using molecular dynamics (MD) simulations. The TC is found to decrease with the increase in graphene layer number from one to three. Further increase in the number of layers has no effect on the TC. The TC is also found to increase monotonously with the temperature in the range from 50 to 300 K. However, there is no effect of temperature on TC beyond 300 K. In order to enhance the TC value, we have investigated the thermal transport in the defect mediated gold−graphene interface for various defect sizes and defect densities. TC is found to increase significantly with the increase in the vacancy defect size and density of defects in the graphene sheet. The TC obtained for graphene containing defects of size 2.24 and 3.16 Å at 300 K is found to be 5 and 26% higher than the TC obtained for defect free graphene. The vibrational density of states (VDOS) of interface forming materials shows that the defects in the graphene sheet enhance the out-of-plane low frequency vibrational modes within graphene. This process facilitates high vibrational coupling between the gold and graphene, and enhances the heat transfer across the interface. This demonstrates that the TC across the gold−graphene interface can be tuned by adjusting the defect vacancy size and density of the defects.

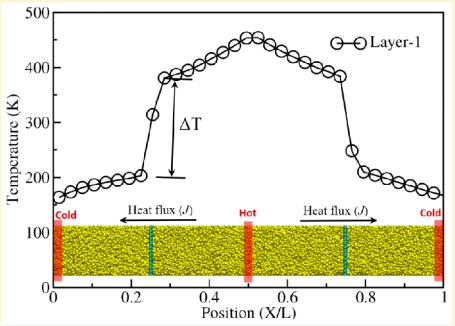

INTRODUCTION

Energy consumption, dissipation, and waste are the main challenges in the modern society. The devices based on nanoscale materials have great potential for the design of energy efficient and high performance applications. The efficiency of these devices is limited by the heat dissipation challenges in the nanoscale integrated circuits. For example, in electronic systems, from the single processor to the data centers, the power dissipation limits the performance.[1] While there is no fundamental physical limitation of the device, the heavy cooling requirement makes the nanoscale device more energy inefficient.[2] The thermal devices made in the last few decades are equipped with advanced heat transfer devices like magnetic thermal switches, heat pipes, and thermoelectrics.[3−5] Even though the heat transfer devices are significantly advanced and efficient, the interfaces of the heat transfer devices and the thermal devices limit the performance.[4] These operational efficiency problems with the present technologies can be addressed by increasing the maximum heat dissipation per unit area through thermal engineering at the nanoscale interfaces. The on-chip power densities in the existing silicon-based microprocessors are typically in the range of 100 $W{\cdot}cm^{-2}$, which is higher than the typical cooling facilities.[2] These high power densities are the major factor, which limits the operating speed of the processor to a few GHz.[2] The remarkable high power densities can result in hot-spot formation and eventual failure of the device. Thus, such a situation is unwanted and an efficient solution is warranted for removing heat generated at the nanometric scale from the devices. Thus, it is necessary to develop a possible means for high thermal conduction in nanodevices to reduce the heat load.

In the modern society, the demand for efficient and low energy consuming devices is steadily increasing, while the requirement of energy from developing countries has increased many folds in recent years.[6−8] Thus, it is of utmost importance to convert the waste heat into useful utility, which is a challenge. This makes the present generation energy issue a two-sided problem. On one side, there is a significant need for novel and energy efficient materials to meet the high energy demands. On the other side, one needs to minimize the effect of these technologies on the environment, in terms of CO_2 emission and global warming. Consequently, understanding and improvement of the energy transport in electronic and computing devices have a long lasting effect.

The electronic devices and systems are constructed using different layers of materials, which include different metals,

Received: September 28, 2017
Revised: December 6, 2017
Published: January 3, 2018

DOI: 10.1021/acs.jpcc.7b09643
J. Phys. Chem. C 2018, 122, 2113−2121

semiconductors, and dielectric substances.[9] Hence, it is imperative to study the interface properties for the development of novel and efficient energy generation and storage devices. The thermal transport across solid interfaces is quantified by the thermal boundary conductance or Kapitza conductance.[10] This quantifies the efficiency of heat transport across the interface. The high thermal conductivity and the surface area of the graphene[11] make it a promising material for heat dissipation applications in nanoelectronic devices. Metal contacts are important in interfacing the graphene in electronic devices. Hence, it is very important to understand the nature of interaction and transport properties across the metal−graphene interfaces. The study of metal contacts with the graphene is important not only because they are an essential part of any active device but also because they are a primary path of heat dissipation.[12] The metal−graphene system properties are expected to be highly dependent on the nature of their interaction and bonding strength. On the basis of bonding nature, the interaction of metals and graphene can be categorized into two types: physisorption and chemisorption.[13] The recent studies on metal−graphene systems demonstrated that physisorption is observed for Ag, Al, Au, Cd, Cu, Ir, and Pt metals with the graphene, whereas chemisorption is observed for Co, Ni, Pd, Ru, and Ti metal−graphene interfaces.[14−16] Sundaram et al.[17] demonstrated that the electronic structure and electron−phonon coupling of graphene are unaltered upon deposition of gold on graphene. The authors also showed that the thermal coupling at the gold−graphene interface plays an important role in thermal management during the electronic device operation. Experiments are also used to estimate the interface thermal resistance across various metal−graphite interfaces (Cu, Al, Ti, and Au,) and the reported thermal resistance values are in the range from 0.8 to 2.5 × 10^{-8} K m^2/W.[18] Various researchers also studied the effect of graphene oxidation[19] and chemical functionalization[20] on graphene−metal interface thermal conductance using experiments. Murad et al.[21,22] used molecular simulations to study the thermal transport across interfaces of silica−water and silica−water in contact with water vapor systems. The authors explained the thermal resistance across the interface on the basis of impedance to the passage of thermal phonons across the interface and hydrophilic nature of the interface. Further, it is also shown that the interface resistance can be manipulated by changing the surface morphology[23] and by changing the interface temperature[24] of solid−liquid systems. Recent studies of various interface thermal transport calculations using molecular dynamics (MD) simulations[25−27] show that the MD simulations can be used to accurately estimate the interface transport properties and the nature of interface interactions. However, thermal transport studies on the graphene−metal interface using MD simulations have received much less attention. There are only very few DFT and MD simulations, which are performed to understand the interactions of metal−graphene interfaces.[14−16,28] As gold is one of the high thermal conductivity metals with a low coefficient of thermal expansion[29] and high corrosion resistance,[30] it has the potential to be used as an interfacing material to address the heat dissipation challenges in nanodevices. Recently, Kaur et al.[31] used a covalently bonded CNT−array−gold nanocomposite on a microchip to enhance the interface thermal conductance. Moreover, the graphene is a high thermal conductivity material, and the thermal conductivity of graphene can be changed by physical and chemical modification. In the recent past, it was also shown that multilayer graphene shows different thermal conductivity than a single graphene sheet.[32,33] The phonon engineering of graphene may make it possible to increase the thermal conductance across the gold−graphene interface. So far, the effect of graphene layer thickness, nanoscale defects in graphene, and temperature on gold−graphene interface thermal transport and related physics is not clear. To address these aspects, we have conducted MD simulations to predict the gold−graphene interface thermal conductance for various graphene layer thicknesses (different numbers of graphene layers) and temperatures. The thermal conductivity of graphene can be changed by physical (creating defects and applying strain) and chemical (functionalization and doping) modification. The phonon engineering of graphene may make it possible to increase the thermal conductance across the gold−graphene interface. The present cooling requirement in electronic and computing devices also warrants the need for enhancing the interface thermal conductance across the metal−graphene interfaces. In this direction, we have studied the effect of defect vacancies in the graphene layer on gold−graphene interface thermal conductance using MD simulations.

This paper is arranged as follows: In the following section, we have presented the model and methodology used to predict the thermal conductance (TC) across the gold−graphene interface. Subsequently, we have presented results and discussions followed by conclusions.

MODEL AND METHODOLOGY

The most common methods used to predict the thermal boundary resistances are the acoustic mismatch model (AMM)[34] and the diffuse mismatch model (DMM).[35] In the AMM method, the material is assumed as continua with a perfect interface with the assumption of phonon scattering at the interface. On the other hand, in the DMM method, a complete diffuse scattering of phonons is assumed, and phonon transmission is completely dependent on the phonon density of states of the materials forming the interface. Further, in both methods, the phonon scattering is assumed to be elastic. It is observed that the conventional DMM method, even with added anisotropy and multiple heat transport mechanisms, substantially underestimates the TC (14.71 MW/m^2·K)[36] across the gold−graphene interface (the experimental value is in the range 30−50 MW/m^2·K).[18,20,37] The Green method[38,39] includes the inelastic scattering effects, but the method is computationally expensive.

The methods based on molecular dynamics (MD) simulations are also used to predict the TC, which do not require any assumptions related to phonon scattering. The direct method[21,22,40−42] and Green−Kubo method[43−45] are usually used to predict the thermal conductivity of a material. For an inhomogeneous system containing a grain boundary, the direct method is preferable. The Green−Kubo method computes the average thermal conductivity over the entire system; thus, it is not suitable to study the interfacial effects.[46] Moreover, the Green−Kubo method suffers from the difficulty of convergence of the heat flux vector and the autocorrelation function. In the direct method, large temperature gradients are required and there is a real interface at the heat sink and source; therefore, finite size effects are expected to be more predominant with this method.[46] The reverse nonequilibrium method (RNEMD) method,[47] on the other hand, has the features of an ideal method, such as no artificial boundaries in the simulation system, compatible with the chosen boundary

DOI: 10.1021/acs.jpcc.7b09643
J. Phys. Chem. C 2018, 122, 2113−2121

conditions, works for small temperature gradients, applicable independently of the chosen ensemble, and reasonably quick compared to the Green−Kubo method.

In this work, the interface thermal boundary conductance of metal−graphene nanocomposites is determined using RNEMD simulations. All of these simulations are performed using the LAMMPS MD simulation package.[48] We have considered a nanocomposite of gold and *n*-layer graphene (n = 1, 2, 3, 4, 5, and 6) and determined the thermal conductance across the gold−graphene interface. To carry out these calculations using MD simulations, accurate interaction potentials are required to address the interactions of the gold and graphene system. The C−C interactions within a graphene are described using the modified Tersoff potential.[49] Additionally, Lennard-Jones (LJ) potentials[50] are used to model the interactions between the carbon atoms of different graphene layers. An embedded-atom-model (EAM) potential[51] is used to describe the interactions between the metal atoms. The gold−graphene interactions are described using the Buckingham potential as shown below

$$U_{ij}^{\mathrm{Buck}} = A_{ij}\exp\left(-\frac{r_{ij}}{\rho_{ij}}\right) - C_{ij}r_{ij}^{-6} \quad (1)$$

where i and j are atomic indexes and A_{ij}, ρ_{ij}, and C_{ij} are parameters. The potential parameters are reported in an earlier work of Namsani et al. (unpublished results), where the potential parameters are derived from quantum level calculations and provide a reasonable approximation for the interaction between the gold and graphene. These parameters are shown to be reproducing the macroscopic properties like the contact angle of gold on the graphene surface and the gold−graphene interlayer distance. This potential is also successfully used by Namsani et al.[52] to study the dewetting of gold film and the process of nanoparticle formation on a graphene surface.

The model simulation system used in this study is as shown in Figure 1. The simulation system consists of two gold−graphene interfaces, which divide the gold region into three parts. The thickness of the gold is fixed to 20 nm in all of the calculations. To perform the thermal boundary conductance calculations, the required equilibrated structures of the gold−graphene system are generated using MD simulations. We have first performed the simulations using the NPT ensemble followed by the NVT ensemble. Each ensemble simulation is conducted for 4 ns. The temperature and pressure are maintained using a Nosé−Hoover thermostat and barostat. The equilibrium structure obtained after NPT and NVT ensemble simulations is used to calculate the interface thermal conductance using RNEMD[47] simulations. In this approach, the momentum of the atoms in hot and cold slabs is exchanged every 50 fs to induce the heat flux across the interface of gold−graphene using the NVE ensemble. A time step of 0.5 fs is used to perform these NVE simulations. The induced heat flux during the course of simulation creates the temperature gradient between the cold and hot slabs. NVE ensemble simulations are performed for 10 ns, and the temperature profile within the nanocomposite is obtained in the heat flux direction. To make sure the temperature profile obtained is at steady state, the temperature profile is computed for every 0.5 ns and found that the slope of the temperature profile does not change with time beyond 6 ns. This converged behavior of the temperature profile within the nanocomposite shows that the system has reached a steady state. After achieving this steady

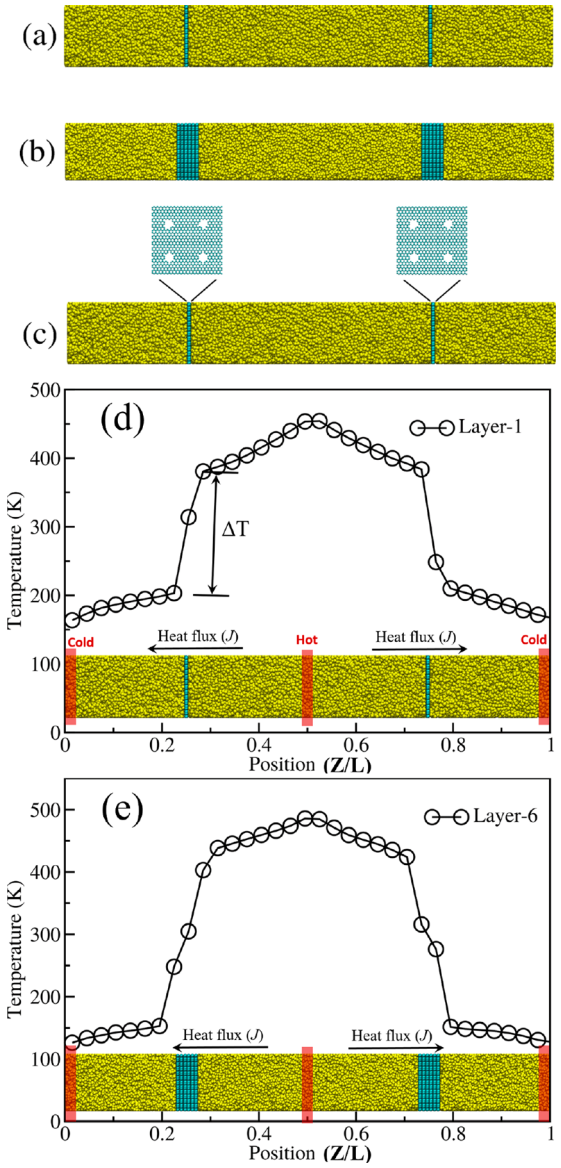

Figure 1. Gold−graphene system with (a) a single graphene sheet, (b) graphene of six layers, and (c) a graphene sheet with four defects. Typical temperature profile within a gold−graphene system at 300 K: (d) single-layer gold−graphene system and (e) six-layer graphene−gold system. The figures shown below the temperature profiles are the model simulation systems used to perform simulations.

state, the temperature jump (ΔT) across the interface of the gold−graphene is computed using the temperature profile obtained. Finally, the obtained temperature change across the interface is used in the below equation to calculate the gold−graphene interface TC.

$$G = \frac{-J_z}{A\Delta T} \quad (2)$$

Here, J_z is the heat flux in the z-direction and A is the cross-sectional area of the nanocomposite. ΔT is the temperature jump across the gold−graphene interface, which can be obtained from the temperature profile.

The gold−graphene interface thermal conductance is predicted for various graphene layer numbers and temperatures using MD simulations. We have also predicted the interface TC by considering graphene with defects. To perform these

DOI: 10.1021/acs.jpcc.7b09643
J. Phys. Chem. C 2018, 122, 2113−2121

calculations, we have created different sizes of vacancy defects by removing carbon atoms from the graphene sheet. We have also varied the number of vacancy defects in graphene to study the effect of defect density on the interface TC.

The underlying mechanism of interfacial thermal transport for the case of nanocomposites formed with the gold and graphene, with and without defects, is investigated by computing the vibrational density of states (VDOS) of interface forming materials, gold, pristine graphene, and graphene with defect vacancies, using MD simulations. VDOS provides the spectral description of the atomic vibration and motion in the system. To compute the VDOS, we first perform 4 ns NPT ensemble simulations to obtain the equilibrium structure, which is used to perform NVT ensemble simulations at desired temperatures for 4 ns. After NVT simulations, an additional 4 ns of NVE ensemble simulations are performed on the equilibrium structure, and velocities of the graphene carbon atoms are sampled for the last 100 ps with an interval of 0.1 ps. The velocity of these atoms is further used to calculate the velocity autocorrelation function, VACF = $\langle v(t)v(0)\rangle$, where v is the velocity of the atom, t is time, and $\langle\ \rangle$ denotes the ensemble average. The Fourier transform of the VACF provides the VDOS, as shown in eq 3.

$$\text{VDOS, } D(\omega) = \frac{1}{\sqrt{2\pi}} \int_0^\infty e^{i\omega t} \left\langle \sum_{i=1}^{N} v_i(t)v_i(0) \right\rangle d\omega \tag{3}$$

In the above equation, $D(\omega)$ is the density of states function. The ω and t are the frequency and time. As the gold−graphene nanocomposite is a combination of dissimilar materials with different phonon transmission mechanisms, the vibrational coupling of the interface forming materials controls the interface TC and this vibrational coupling is quantified using the overlap factor. The overlap of the VDOS for the interface forming with gold and graphene is defined using the equation given below[53]

$$S = \frac{\int_0^\infty D_c(\omega)D_g(\omega)\, d\omega}{\int_0^\infty D_c(\omega)\, d\omega \int_0^\infty D_g(\omega)\, d\omega} \tag{4}$$

where S is the overlap factor and subscripts c and g of $D(\omega)$ indicate the VDOS of carbon and gold, respectively.

RESULTS AND DISCUSSION

The interface TC for the gold−graphene system is determined for different graphene layer thicknesses (layer number) at different temperatures. The typical temperature profiles obtained for a single-layer and six-layer gold−graphene system at 300 K are shown in Figure 1d and e, respectively. These figures clearly show a jump in the temperature profile at the gold−graphene interface. The temperature jump (ΔT) across the interface is indicative of the resistance offered by the interface for thermal transport. This ΔT across the interface and the flux induced in the system are used to predict the TC across the interface (see eq 2). Parts d and e of Figure 1 also clearly show that ΔT is more for a six-layered nanocomposite compared to the single-layer nanocomposite.

The thermal conductivity of multilayer graphene is shown to be lower than the single-layer graphene.[32] It was also shown that the use of graphene and a multilayer graphene mixture in a thermal material matrix enhances the thermal conductivity by several folds compared to the single-layer graphene.[33] Lee et al.[54] reported a decrease in the SERS enhancement with an increase in graphene layer thickness for Ag−graphene nanocomposites. This shows that the graphene layer thickness affects the electronic and thermal properties. Thus, it is important to know the effect of graphene layer thickness on gold−graphene interface TC.

Figure 2 shows the change in interface TC with the graphene layer number and temperature. The TC calculations are performed for gold−graphene systems containing different numbers of graphene layers (n = 1 to 6) in the temperature range from 50 to 700 K. These results demonstrate that TC increases with the temperature in the range 50−300 K. After 300 K, the TC does not change with the temperature. This shows that the TC is insensitive to the temperature change beyond 300 K. Figure 2 also shows the decrease in the TC with the increase in graphene layer number from 1 to 3. Beyond three layers, the TC is found to be insensitive to the change in layer number.

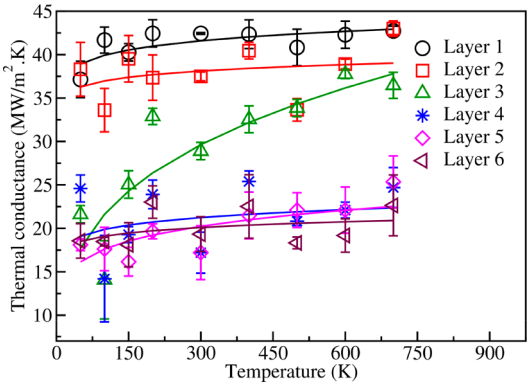

Figure 2. Thermal conductivity as a function of temperature for different layers of graphene. The solid lines are average trend lines.

The computed thermal conductances across a single-layer gold−graphene interface at 50 and 300 K are 36.6 and 42.0 MW/m^2·K, respectively. The TC obtained at 300 K (42.04 MW/m^2·K) for the single-layer graphene is in good agreement with the values reported in experiments (30−50 MW/m^2·K).[18,20,37] The DFT calculated value (58.82 MW/m^2·K)[12] is higher than the values from this work and that in the experiments. This is mainly because the DFT study did not include the van der Waals interaction completely, which is the main interaction between the gold and graphene. On the other hand, it is observed that the conventional diffusive mismatch models, even with added anisotropy and multiple heat transport mechanisms, substantially underestimate the TC across the Au/Gr interface (14.71 MW/m^2·K).[36] The increase in TC is 14.6% with the change in temperature from 50 to 300 K. In case of the two-layer graphene system, increasing the temperature from 50 to 300 K increases the TC by 36.9%. At 300 K, the TC of the two-layer graphene system is 38 MW/m^2·K. This is almost 10% less than the TC observed for the single-layer graphene system. In the case of the three-layer graphene system, the TC increases by 52% with the increase in temperature from 50 to 300 K. However, the TC in the case of the three-layer system is 37.7% less than that of the single-layer graphene system at 300 K. For the three-layer system, Figure 2 shows that below 300 K there is a suppression of phonon transport in the heat flux direction, and as we increase the temperature, there is an enhancement in the thermal conductance. Below 300 K, we observe ripple

DOI: 10.1021/acs.jpcc.7b09643
J. Phys. Chem. C 2018, 122, 2113−2121

formation, in which graphene atoms move in the perpendicular direction to the heat flow (see parts a and b of Figure S1 in the Supporting Information, which clearly show structural changes at low (T = 250 K) and high temperatures (T = 700 K)). The ripples observed at lower temperatures diminish with an increase in temperature. At higher temperatures, the thermal motion of the gold is high, which suppresses the layer motion and enhances the intermolecular collision frequency at the interface. In other words, high temperature promotes enhanced heat transport across the gold−graphene interface. After three layers, there is no significant change in the TC with the layer number. This decrease in the heat transport with increasing layer numbers is also in agreement with the behavior observed in a system consisting of a varying number of Si and silicon-like nanolayers and water interfaces.[55]

In the recent years, many authors showed that thermal transport in graphene can be modified by means of physical or chemical modification of the surface. In general, the physical modification involves applying strain, creating defects and nanopores. All of these physical modifications are shown to affect the phonon transport in the graphene sheet. Murad et al.[23] showed that the interface heat transport can be manipulated by changing the surface morphology at the solid−fluid interface. It was shown by them that inhomogeneous solids could be used to design the thermal rectifiers.[56,57] Various authors[58,59] also showed that tuning the surface charge, morphology, and adsorbed moieties could enhance the thermal conductivity of nanofluids and the thermal conductance of solid−solid interfaces. Huang et al.[60] showed that the annealing induced topological conformity enhances the TC across the metal−graphene interface. However, to the best of our knowledge, the effect of topological defects on the metal−graphene interface thermal conductance is not studied. In this study, we have used a graphene sheet with vacancy defects in place of normal graphene and estimated the TC across the gold−graphene interface. We have considered two defect sizes to study the effect of these nanodefects on TC across the gold−graphene interface. The sizes of the defects created in a graphene sheet are 2.24 and 3.16 Å. The number of defects (N) in the graphene sheet was also varied (N = 1, 2, 4, and 9) to study the effect of defect density on TC across the gold−graphene interface. For the case of defect free graphene, the obtained TC at 300 K across the gold−graphene interface is ∼42 MW/m^2·K, which is higher than the values observed below 300 K (see Figure 3a) for the single layer. In order to understand the effect of temperature on the interface TC for different defect densities, we varied the temperature from 50 to 300 K. The variation in interface TC with temperature for the case of the defect size 2.24 Å is shown in Figure 3a.

From the above figure, it is evident that the TC increases with the temperature for both cases, viz., graphene with defects and graphene without defects. Moreover, the TC obtained for the system of graphene containing defects is higher compared to the defect free graphene. For the gold−graphene system containing graphene with defects, the TC is found to increase with the number of defects from 1 to 9 (N = 1−9). The obtained TC at 300 K for graphene containing N = 9 is ∼44 MW/m^2·K, which is 4.8% higher than the TC obtained for the defect free graphene, at the same temperature. The TC obtained for N = 9 is 7.8, 3.5, and 2.2% higher than the TC obtained for N = 1, 2, and 4, respectively. This behavior is consistent with the recent experimental investigations of Kim et al.,[61] where they have reported an increase in TC of graphene−Cu/Al interfaces with the increase in the percentage of defects. In all cases, for a given number of defects, the TC is found to be highest at 300 K.

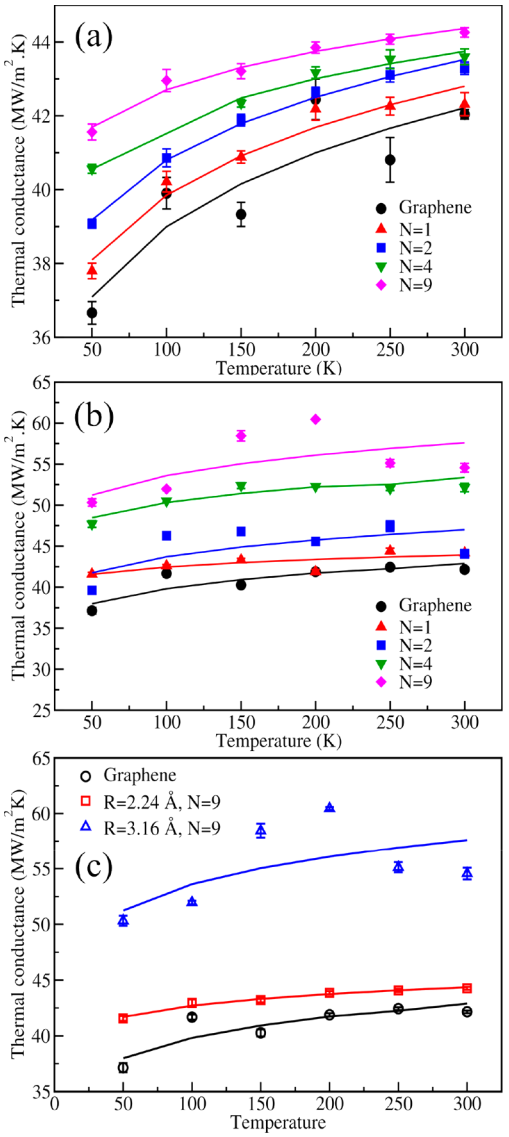

Figure 3. (a) Variation in TC with the temperature and defect density for the case of graphene containing a defect of size 2.24 Å. (b) Same as in part a but with a defect of size 3.16 Å. (c) Variation in TC with the temperature and defect size. The solid lines are average trend lines.

Next, we study the effect of defect size on TC. The variation in TC with the temperature and defect density for the case of 3.16 Å defect size is shown in Figure 3b. The TC is found to increase with increasing temperature for graphene with N = 1, 2, 4, and 9. The increase in the number of defects in graphene also enhances the TC of the gold−graphene interface. The obtained interface TC for N = 9 at 300 K is ∼53 MW/m^2·K. This value is 26% more than the TC of defect free graphene at the same temperature. The percentage of increase in TC for graphene containing N = 9 is 25, 23, and 6% when compared with the obtained TC for graphene containing 1, 2, and 4 defects, respectively.

In order to provide a clear understanding of the effect of defect size on interface TC, we have shown the TC obtained for graphene containing N = 9 for both defect sizes (2.24 and 3.16 Å) along with the TC of defect free graphene in Figure 3c.

DOI: 10.1021/acs.jpcc.7b09643
J. Phys. Chem. C 2018, 122, 2113−2121

The TC obtained for graphene containing nine defects of size 2.24 and 3.16 Å is 4.8 and 26% higher than the TC obtained for defect free graphene at 300 K. The TC obtained for graphene containing nine defects of size 3.16 Å is 20% higher than the TC obtained for the case of graphene containing nine defects of size 2.24 Å. This clearly shows that at a given temperature the increase in defect size increases the TC.

The above results clearly show that the TC across the gold−graphene is enhanced with the creation of nanoscale defects in graphene. The defect-containing graphene exhibits better thermal conductance compared to the graphene without defects. For example, various authors[62−64] using DFT calculations showed enhanced adsorption characteristics for defective graphene and metal (gold, Pt, Fe, and Al) nanoparticles through binding energy calculations. The increase in adsorption of the gold at the gold−graphene interface enhances the intermolecular collision frequency and facilitates high heat transport. This type of increase in the thermal conduction behavior is also observed for hydrophilic interfaces of the Si−water system with water vapor.[22] The enhancement in the gold−graphene thermal conductance with the created defects in graphene may be attributed to the change in the vibrational coupling between the gold and graphene materials.

In order to gain a detailed understanding of the heat flow across the gold−graphene interface, we analyze the vibrational characteristics of the materials forming the interface. This is achieved by first calculating the velocity autocorrelation function (VACF) of the interface materials. The Fourier transform of this VACF is known as the vibrational density of states (VDOS). The thermal transport across the interface is dependent on the vibrational coupling between the materials forming the interface. The overlap of VDOS for the interface forming materials controls the thermal transport across the interface. Thus, the concept of overlap of VDOS has been used effectively to address phonon thermal transport in many systems, viz., asymmetric graphene nanoribbons,[65] bilayer nanofilms,[66] graphene−SiC,[67] and graphene−hBN nanoribbons.[68] In practice, the overlap of VDOS is represented by an overlap factor (S), which is calculated using eq 4. In this work, the overlap factor, S, is a qualitative measure for the phonon−phonon coupling between the gold and graphene at the interface.

In all cases, the out-of-plane low frequency part of the vibrational spectra at 300 K is shown because these low frequency vibrations are responsible for the majority of heat transfer across the interface. The high frequency in-plane vibrations do not contribute much to the interface thermal transport.[25] The VDOS profiles obtained for gold and multilayer graphene are shown Figure 4a. The gold vibrational spectra show that the gold vibrational modes are of low frequency in nature and the vibrational frequency is in the range from 0 to 10 THz. On the other hand, the VDOS of graphene and multilayer graphene show vibrational modes in the high frequency domain ranging from 0 to 50 THz. To have a better vibrational coupling with gold, the contact material at the interface should have vibrational frequency in the same range as gold. As the gold atom vibrational frequency is below 10 THZ (see Figure 4a), comparison of the VDOS of multilayer graphene and graphene containing defects within this range of frequency addresses the change in thermal conductance. From the profiles of gold and graphene shown in Figure 4a, it is evident that there is no overlap of the VDOS of graphene and gold except in the range from 0 to 10 THz. This

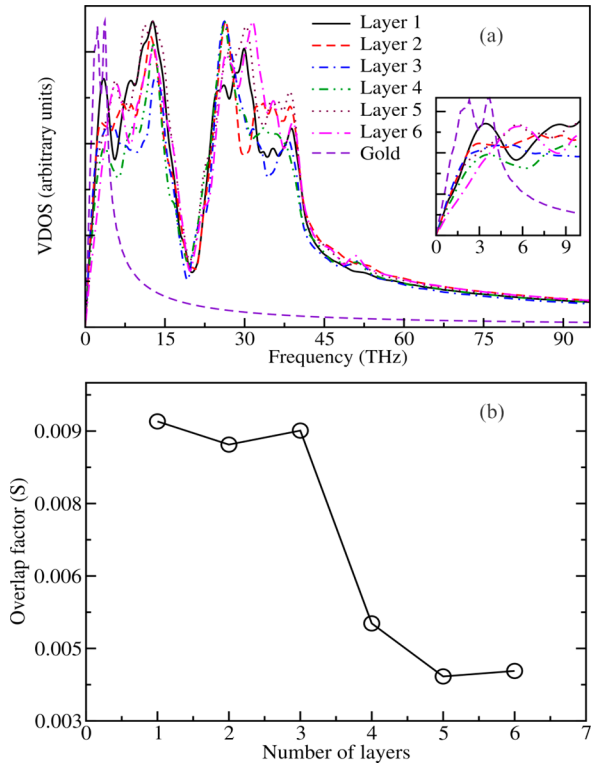

Figure 4. (a) VDOS profiles for n-layer graphene (n = 1−6) and gold. (b) Overlap factor obtained for different numbers of graphene layers with gold VDOS.

indicates potentially a high resistance for the heat transfer across the gold−graphene interface. In Figure 4a, we have shown the zoomed in view of the VDOS of defect free graphene and graphene containing defects, within the 10 THz frequency range, as an inset.

The inset in Figure 4a clearly shows that with the increase in graphene layer number the phonon vibrational modes shift toward the high frequency side. This results in substantial VDOS overlap for single-layer graphene and gold compared to the other multilayer graphene systems. The VDOS overlap can be quantified using the overlap factor (S), which is shown in Figure 4b. From this figure, we can clearly see that the single-layer graphene shows more overlap compared to other multilayer graphene systems. The overlap factor is found to be decreasing with the increase in the layer number. This shows the decrease in vibrational coupling with the increase in layer number. The percentage of decrease in vibrational coupling is 3.2, 2.1, 43.4, 72, and 72% for two-, three-, four-, five-, and six-layer graphene, respectively. This clearly shows that the TC decreases up to a graphene layer number of 3. Further increase in the number of layers has no visible effect on the TC, which is also observed in the interface TC calculations (see Figure 2).

Figure 5a displays the VDOS for pristine graphene and graphene containing N = 2 and 9 defects, of size 2.24 Å, at 300 K. The VDOS profiles for graphene containing N = 1, 2, 4, and 9 defects of size 2.24 and 3.16 Å along with the VDOS profile for defect free graphene are shown in Figure S2 and Figure S3, respectively (see the Supporting Information). The gold and defect free graphene VDOS are also shown in Figure 5a for comparison. The VDOS profile for graphene shows that the phonon mode distribution is broader toward high frequency. For N = 2, graphene containing two defects, the VDOS

DOI: 10.1021/acs.jpcc.7b09643
J. Phys. Chem. C 2018, 122, 2113−2121

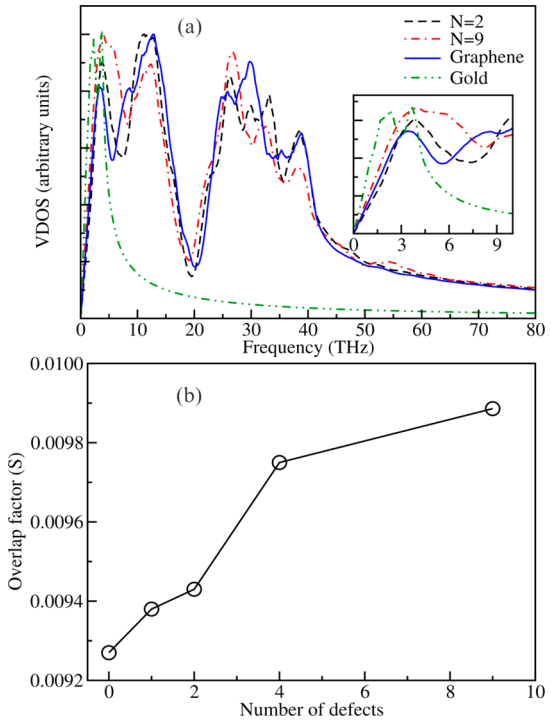

Figure 5. (a) VDOS profiles for defect free graphene, graphene with defects (N = 2 and 9), and gold; the inset shows the zoomed in view of VDOS within 10 THz. (b) Variation of gold−graphene VDOS overlap factor with the number of defects in graphene.

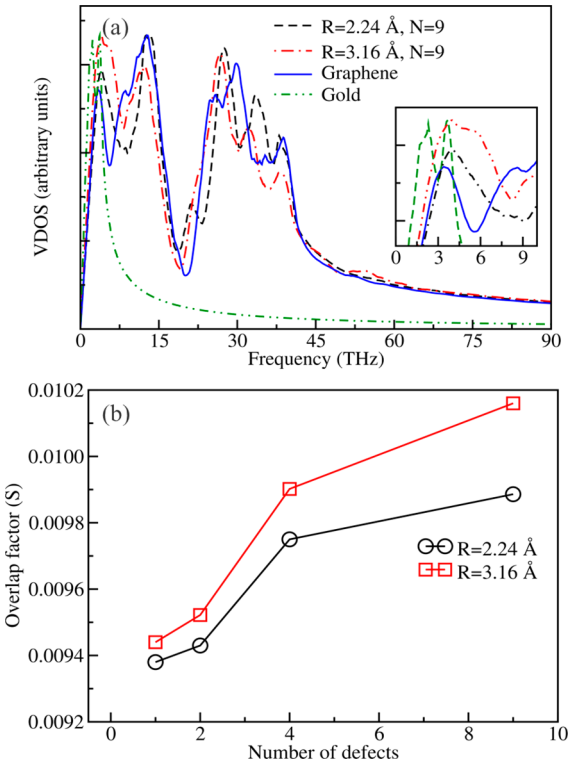

Figure 6. (a) VDOS profiles for gold, defect free graphene, and graphene containing nine defects of size 2.24 and 3.16 Å; the inset shows the zoomed in view of the VDOS within 10 THz. (b) Variation of gold−graphene VDOS overlap factor with the number of defects in graphene for pore size 2.24 and 3.16 Å.

distribution peak width increases toward the low frequency compared to the defect free graphene. This shows that the phonon modes are shifted toward the lower frequency with the defect creation within the graphene sheet. As the number of defects increases from N = 2 to N = 9, the phonon distribution width gets broader toward the lower frequency (toward 5 THz). The shift of these vibrational modes is quantified using the overlap factor, and the obtained overlap factors are shown in Figure 5b. It is evident from the figure that the overlap factor increases with the increase in defect density. We have also observed a similar kind of VDOS behavior for the case of graphene containing defects of size 3.16 Å (see Figures S4a and b in the Supporting Information). This clearly shows that the graphene with defects exhibits better vibrational coupling with gold than the defect free graphene. This increase in vibrational coupling results in lower resistance at the interface and offers high heat flow across the interface. This behavior of an increase in interface TC is also clearly shown in Figure 3a and b.

Furthermore, to illustrate the change in VDOS with the change in defect size, the VDOS for graphene containing N = 9 defects of size 2.24 and 3.16 Å is shown in Figure 6a along with the VDOS of defect free graphene and gold.

Figure 6a shows that the dominant vibrational modes in graphene, observed at 15 and 33 THz, are shifted toward the lower frequency side upon introducing the defects. For better thermal transport across the gold−graphene interface, the enhancement of lower vibrational modes within the range of gold VDOS is required. The zoomed in view of VDOS within the gold vibrational range (0−10 THz) is shown as an inset in Figure 6a. This clearly shows that the graphene with defects exhibits more overlap in VDOS with gold compared to defect free graphene. Moreover, the increase in defect size further increases the overlap of VDOS with gold. The overlap factor obtained for both defect sizes with the increase in defect density is shown in Figure 6b. The overlap factor for both defect sizes increases with an increase in the number of defects. It is also evident that for a given number of defects the graphene with 3.16 Å size defects shows more VDOS overlap with gold compared to the graphene containing 2.24 Å size defects. The above results clearly demonstrate that the increase in the number of defects and the increase in the defect size in graphene enhances the thermal transport across the gold−graphene interface. This observation is also in line with the interface TC calculations shown in Figures 2, 3a, and 3b.

CONCLUSIONS

We have studied the thermal transport across the gold−graphene interface and explored the mechanism of thermal transport using MD simulations. The TC is found to increase with an increase in the number of graphene layers up to three. For more than three layers of graphene, we do not observe any change in TC. Furthermore, we have studied the thermal transport in the defect mediated gold−graphene system. The results demonstrate that introducing defects in the graphene sheet enhances the TC across the interface. The obtained TC at 300 K for a graphene sheet with N = 9 of size 2.24 and 3.16 Å shows 4.8 and 26% enhancement, compared to defect free graphene, respectively. This shows that the increase in defect size and defect density enhances the TC. The TC obtained for the case of graphene with and without defects in the temperature range from 50 to 300 K demonstrates that the TC increases with an increase in temperature. Further, the VDOS shows that the defects in the graphene sheet enhance the out-of-plane low frequency vibrational modes and facilitate

DOI: 10.1021/acs.jpcc.7b09643
J. Phys. Chem. C 2018, 122, 2113−2121

better vibrational coupling between the graphene and gold. The vibrational coupling between the gold and graphene is quantified using the overlap factor. The overlap factor obtained for both graphene with and without defects shows more overlap of VDOS for graphene containing defects compared to defect free graphene. Moreover, we have found that the overlap factor increases with the increase in defect size and defect density, which is line with the behavior seen in computed TC. The increase in the number of defects and defect size increases the adsorption of the graphene layer on the gold interface, which enhances the intermolecular collision frequency at the interface. The enhanced intermolecular collisions at the interface reduce the resistance to the passage of the thermal phonons across the gold−graphene interface. This concludes that the increase in defect size and defect density enhances the vibrational coupling between gold and graphene, which results in enhancement of thermal transport across the interface.

■ ASSOCIATED CONTENT

Supporting Information

The Supporting Information is available free of charge on the ACS Publications website at DOI: 10.1021/acs.jpcc.7b09643.

Snapshots of the three-layer gold−graphene system at 300 and 700 K and the vibrational density of states (VDOS) for all of the defects of the graphene−gold systems considered in this study (PDF)

■ AUTHOR INFORMATION

Corresponding Author

*E-mail: jayantks@iitk.ac.in.

ORCID

Jayant K. Singh: 0000-0001-8056-2115

Notes

The authors declare no competing financial interest.

■ ACKNOWLEDGMENTS

The High Performance Computing (HPC) facility of Indian Institute of Technology Kanpur is gratefully acknowledged. This work was supported by SERB, Department of Science and Technology, Government of India.

■ REFERENCES

(1) Pop, E. Energy Dissipation and Transport in Nanoscale Devices. *Nano Res.* **2010**, *3*, 147−169.

(2) Pop, E.; Sinha, S.; Goodson, K. E. Heat Generation and Transport in Nanometer-Scale Transistors. *Proc. IEEE* **2006**, *94*, 1587−1601.

(3) Zhang, Y.; Du, Y.; Shum, C.; Cai, B.; Le, N. C. H.; Chen, X.; Duck, B.; Fell, C.; Zhu, Y.; Gu, M. Efficiently-Cooled Plasmonic Amorphous Silicon Solar Cells Integrated with a Nano-Coated Heat-Pipe Plate. *Sci. Rep.* **2016**, *6*, 24972.

(4) Chowdhury, I.; Prasher, R.; Lofgreen, K.; Chrysler, G.; Narasimhan, S.; Mahajan, R.; Koester, D.; Alley, R.; Venkatasubramanian, R. On-Chip Cooling by Superlattice-Based Thin-Film Thermoelectrics. *Nat. Nanotechnol.* **2009**, *4*, 235−238.

(5) Puga, J. B.; Bordalo, B. D.; Silva, D. J.; Dias, M. M.; Belo, J. H.; Araújo, J. P.; Oliveira, J. C. R. E.; Pereira, A. M.; Ventura, J. Novel Thermal Switch Based on Magnetic Nanofluids with Remote Activation. *Nano Energy* **2017**, *31*, 278−285.

(6) Forshaw, M.; Stadler, R.; Crawley, D.; Nikolić, K. A Short Review of Nanoelectronic Architectures. *Nanotechnology* **2004**, *15*, S220.

(7) Goldhaber-Gordon, D.; Montemerlo, M. S.; Love, J. C.; Opiteck, G. J.; Ellenbogen, J. C. Overview of Nanoelectronic Devices. *Proc. IEEE* **1997**, *85*, 521−540.

(8) Poulikakos, D.; Maruyama, S. Review. *Microscale Thermophys. Eng.* **2003**, *7*, 181−206.

(9) He, M.; Lu, T.-M. *Metal-Dielectric Interfaces in Gigascale Electronics*, 1st ed.; Springer-Verlag: New York, 2012.

(10) Kapitza, P. L. Heat Transfer and Superfluidity of Helium Ii. *Phys. Rev.* **1941**, *60*, 354−355.

(11) Novoselov, K. S.; Falko, V. I.; Colombo, L.; Gellert, P. R.; Schwab, M. G.; Kim, K. A Roadmap for Graphene. *Nature* **2012**, *490*, 192−200.

(12) Mao, R.; Kong, B. D.; Gong, C.; Xu, S.; Jayasekera, T.; Cho, K.; Kim, K. W. First-Principles Calculation of Thermal Transport in Metal/Graphene Systems. *Phys. Rev. B: Condens. Matter Mater. Phys.* **2013**, *87*, 165410.

(13) Khomyakov, P. A.; Giovannetti, G.; Rusu, P. C.; Brocks, G.; van den Brink, J.; Kelly, P. J. First-Principles Study of the Interaction and Charge Transfer between Graphene and Metals. *Phys. Rev. B: Condens. Matter Mater. Phys.* **2009**, *79*, 195425.

(14) Ran, Q.; Gao, M.; Guan, X.; Wang, Y.; Yu, Z. First-Principles Investigation on Bonding Formation and Electronic Structure of Metal-Graphene Contacts. *Appl. Phys. Lett.* **2009**, *94*, 103511.

(15) Gong, C.; Lee, G.; Shan, B.; Vogel, E. M.; Wallace, R. M.; Cho, K. First-Principles Study of Metal−Graphene Interfaces. *J. Appl. Phys.* **2010**, *108*, 123711.

(16) Gong, C.; Hinojos, D.; Wang, W.; Nijem, N.; Shan, B.; Wallace, R. M.; Cho, K.; Chabal, Y. J. Metal−Graphene−Metal Sandwich Contacts for Enhanced Interface Bonding and Work Function Control. *ACS Nano* **2012**, *6*, 5381−5387.

(17) Sundaram, R. S.; Steiner, M.; Chiu, H.-Y.; Engel, M.; Bol, A. A.; Krupke, R.; Burghard, M.; Kern, K.; Avouris, P. The Graphene−Gold Interface and Its Implications for Nanoelectronics. *Nano Lett.* **2011**, *11*, 3833−3837.

(18) Schmidt, A. J.; Collins, K. C.; Minnich, A. J.; Chen, G. Thermal Conductance and Phonon Transmissivity of Metal−Graphite Interfaces. *J. Appl. Phys.* **2010**, *107*, 104907.

(19) Jiang, T.; Zhang, X.; Vishwanath, S.; Mu, X.; Kanzyuba, V.; Sokolov, D. A.; Ptasinska, S.; Go, D. B.; Xing, H. G.; Luo, T. Covalent Bonding Modulated Graphene-Metal Interfacial Thermal Transport. *Nanoscale* **2016**, *8*, 10993−11001.

(20) Hopkins, P. E.; Baraket, M.; Barnat, E. V.; Beechem, T. E.; Kearney, S. P.; Duda, J. C.; Robinson, J. T.; Walton, S. G. Manipulating Thermal Conductance at Metal−Graphene Contacts Via Chemical Functionalization. *Nano Lett.* **2012**, *12*, 590−595.

(21) Murad, S.; Puri, I. K. Thermal Transport across Nanoscale Solid-Fluid Interfaces. *Appl. Phys. Lett.* **2008**, *92*, 133105.

(22) Murad, S.; Puri, I. K. Molecular Simulation of Thermal Transport across Hydrophilic Interfaces. *Chem. Phys. Lett.* **2008**, *467*, 110−113.

(23) Murad, S.; Puri, I. K. Communication: Thermal Rectification in Liquids by Manipulating the Solid-Liquid Interface. *J. Chem. Phys.* **2012**, *137*, 081101.

(24) Murad, S.; Puri, I. K. Thermal Transport through a Fluid−Solid Interface. *Chem. Phys. Lett.* **2009**, *476*, 267−270.

(25) Patel, H. A.; Garde, S.; Keblinski, P. Thermal Resistance of Nanoscopic Liquid−Liquid Interfaces: Dependence on Chemistry and Molecular Architecture. *Nano Lett.* **2005**, *5*, 2225−2231.

(26) Luo, T.; Lloyd, J. R. Enhancement of Thermal Energy Transport across Graphene/Graphite and Polymer Interfaces: A Molecular Dynamics Study. *Adv. Funct. Mater.* **2012**, *22*, 2495−2502.

(27) Liu, Y.; Hu, C.; Huang, J.; Sumpter, B. G.; Qiao, R. Tuning Interfacial Thermal Conductance of Graphene Embedded in Soft Materials by Vacancy Defects. *J. Chem. Phys.* **2015**, *142*, 244703.

(28) Chang, S.-W.; Nair, A. K.; Buehler, M. J. Geometry and Temperature Effects of the Interfacial Thermal Conductance in Copper− and Nickel−Graphene Nanocomposites. *J. Phys.: Condens. Matter* **2012**, *24*, 245301.

DOI: 10.1021/acs.jpcc.7b09643
J. Phys. Chem. C 2018, 122, 2113−2121

(29) Chung, D. D. L. Materials for Thermal Conduction. *Appl. Therm. Eng.* **2001**, *21*, 1593−1605.
(30) Young, D. J. Chapter 3 - Oxidation of Pure Metals. In *High Temperature Oxidation and Corrosion of Metals*, 2nd ed.; Elsevier: 2016; pp 85−144.
(31) Kaur, S.; Raravikar, N.; Helms, B. A.; Prasher, R.; Ogletree, D. F. Enhanced Thermal Transport at Covalently Functionalized Carbon Nanotube Array Interfaces. *Nat. Commun.* **2014**, *5*, 3082.
(32) Wei, Z.; Ni, Z.; Bi, K.; Chen, M.; Chen, Y. In-Plane Lattice Thermal Conductivities of Multilayer Graphene Films. *Carbon* **2011**, *49*, 2653−2658.
(33) Shahil, K. M. F.; Balandin, A. A. Thermal Properties of Graphene and Multilayer Graphene: Applications in Thermal Interface Materials. *Solid State Commun.* **2012**, *152*, 1331−1340.
(34) Little, W. A. The Transport of Heat between Dissimilar Solids at Low Temperatures. *Can. J. Phys.* **1959**, *37*, 334−349.
(35) Swartz, E. T.; Pohl, R. O. Thermal Boundary Resistance. *Rev. Mod. Phys.* **1989**, *61*, 605−668.
(36) Duda, J. C.; Hopkins, P. E.; Beechem, T. E.; Smoyer, J. L.; Norris, P. M. Inelastic Phonon Interactions at Solid−Graphite Interfaces. *Superlattices Microstruct.* **2010**, *47*, 550−555.
(37) Zhang, C.; et al. Electron Contributions to the Heat Conduction across Au/Graphene/Au Interfaces. *Carbon* **2017**, *115*, 665−671.
(38) Mingo, N. *Thermal Nanosystems and Nanomaterials*; Springer Science & Business Media: 2009; Vol. *118*.
(39) Mingo, N.; Yang, L. Phonon Transport in Nanowires Coated with an Amorphous Material: An Atomistic Green's Function Approach. *Phys. Rev. B: Condens. Matter Mater. Phys.* **2003**, *68*, 245406.
(40) Hoover, W. G. *Computational Statistical Mechanics*; Elsevier: 2012.
(41) Maiti, A.; Mahan, G. D.; Pantelides, S. T. Dynamical Simulations of Nonequilibrium Processes — Heat Flow and the Kapitza Resistance across Grain Boundaries. *Solid State Commun.* **1997**, *102*, 517−521.
(42) Oligschleger, C.; Schön, J. C. Simulation of Thermal Conductivity and Heat Transport in Solids. *Phys. Rev. B: Condens. Matter Mater. Phys.* **1999**, *59*, 4125−4133.
(43) Che, J.; Çağın, T.; Deng, W.; Goddard, W. A. Thermal Conductivity of Diamond and Related Materials from Molecular Dynamics Simulations. *J. Chem. Phys.* **2000**, *113*, 6888−6900.
(44) Volz, S. G.; Chen, G. Molecular-Dynamics Simulation of Thermal Conductivity of Silicon Crystals. *Phys. Rev. B: Condens. Matter Mater. Phys.* **2000**, *61*, 2651−2656.
(45) Ladd, A. J. C.; Moran, B.; Hoover, W. G. Lattice Thermal Conductivity: A Comparison of Molecular Dynamics and Anharmonic Lattice Dynamics. *Phys. Rev. B: Condens. Matter Mater. Phys.* **1986**, *34*, 5058−5064.
(46) Schelling, P. K.; Phillpot, S. R.; Keblinski, P. Comparison of Atomic-Level Simulation Methods for Computing Thermal Conductivity. *Phys. Rev. B: Condens. Matter Mater. Phys.* **2002**, *65*, 144306.
(47) Muller-Plathe, F. A Simple Nonequilibrium Molecular Dynamics Method for Calculating the Thermal Conductivity. *J. Chem. Phys.* **1997**, *106*, 6082−6085.
(48) Plimpton, S. Fast Parallel Algorithms for Short-Range Molecular Dynamics. *J. Comput. Phys.* **1995**, *117*, 1−19.
(49) Lindsay, L.; Broido, D. A. Optimized Tersoff and Brenner Empirical Potential Parameters for Lattice Dynamics and Phonon Thermal Transport in Carbon Nanotubes and Graphene. *Phys. Rev. B: Condens. Matter Mater. Phys.* **2010**, *81*, 205441.
(50) Girifalco, L. A.; Hodak, M.; Lee, R. S. Carbon Nanotubes, Buckyballs, Ropes, and a Universal Graphitic Potential. *Phys. Rev. B: Condens. Matter Mater. Phys.* **2000**, *62*, 13104−13110.
(51) Grochola, G.; Russo, S. P.; Snook, I. K. On Fitting a Gold Embedded Atom Method Potential Using the Force Matching Method. *J. Chem. Phys.* **2005**, *123*, 204719.
(52) Namsani, S.; Singh, J. K. Dewetting Dynamics of a Gold Film on Graphene: Implications for Nanoparticle Formation. *Faraday Discuss.* **2016**, *186*, 153−170.
(53) Li, B.; Lan, J.; Wang, L. Interface Thermal Resistance between Dissimilar Anharmonic Lattices. *Phys. Rev. Lett.* **2005**, *95*, 104302.
(54) Lee, J.; Novoselov, K. S.; Shin, H. S. Interaction between Metal and Graphene: Dependence on the Layer Number of Graphene. *ACS Nano* **2011**, *5*, 608−612.
(55) Murad, S.; Puri, I. K. Thermal Transport through Superlattice Solid-Solid Interfaces. *Appl. Phys. Lett.* **2009**, *95*, 051907.
(56) Murad, S.; Puri, I. K. Thermal Rectification in a Fluid Reservoir. *Appl. Phys. Lett.* **2012**, *100*, 121901.
(57) Murad, S.; Puri, I. K. A Thermal Logic Device Based on Fluid-Solid Interfaces. *Appl. Phys. Lett.* **2013**, *102*, 193109.
(58) Anbumozhi Angayarkanni, S.; Philip, J. Role of Surface Charge, Morphology, and Adsorbed Moieties on Thermal Conductivity Enhancement of Nanofluids. *Appl. Phys. Lett.* **2012**, *101*, 173113.
(59) Zhang, P.; Cui, T.; Li, Q. Effect of Surface Roughness on Thermal Contact Resistance of Aluminium Alloy. *Appl. Therm. Eng.* **2017**, *121*, 992−998.
(60) Huang, B.; Koh, Y. K. Improved Topological Conformity Enhances Heat Conduction across Metal Contacts on Transferred Graphene. *Carbon* **2016**, *105*, 268−274.
(61) Kim, J.; Khan, M. E.; Ko, J.-H.; Kim, J. H.; Lee, E.-S.; Suh, J.; Wu, J.; Kim, Y.-H.; Park, J. Y.; Lyeo, H.-K. Bimodal Control of Heat Transport at Graphene−Metal Interfaces Using Disorder in Graphene. *Sci. Rep.* **2016**, *6*, 34428.
(62) Zhou, M.; Zhang, A.; Dai, Z.; Zhang, C.; Feng, Y. P. Greatly Enhanced Adsorption and Catalytic Activity of Au and Pt Clusters on Defective Graphene. *J. Chem. Phys.* **2010**, *132*, 194704.
(63) Lim, D.-H.; Negreira, A. S.; Wilcox, J. Dft Studies on the Interaction of Defective Graphene-Supported Fe and Al Nanoparticles. *J. Phys. Chem. C* **2011**, *115*, 8961−8970.
(64) Fampiou, I.; Ramasubramaniam, A. Binding of Pt Nanoclusters to Point Defects in Graphene: Adsorption, Morphology, and Electronic Structure. *J. Phys. Chem. C* **2012**, *116*, 6543−6555.
(65) Wang, Y.; Vallabhaneni, A.; Hu, J.; Qiu, B.; Chen, Y. P.; Ruan, X. Phonon Lateral Confinement Enables Thermal Rectification in Asymmetric Single-Material Nanostructures. *Nano Lett.* **2014**, *14*, 592−596.
(66) Ju, S.; Liang, X.; Wang, S. Investigation of Interfacial Thermal Resistance of Bi-Layer Nanofilms by Nonequilibrium Molecular Dynamics. *J. Phys. D: Appl. Phys.* **2010**, *43*, 085407.
(67) Li, M.; Zhang, J.; Hu, X.; Yue, Y. Thermal Transport across Graphene/Sic Interface: Effects of Atomic Bond and Crystallinity of Substrate. *Appl. Phys. A: Mater. Sci. Process.* **2015**, *119*, 415−424.
(68) Medrano Sandonas, L.; Cuba-Supanta, G.; Gutierrez, R.; Dianat, A.; Landauro, C. V.; Cuniberti, G. Enhancement of Thermal Transport Properties of Asymmetric Graphene/Hbn Nanoribbon Heterojunctions by Substrate Engineering. *Carbon* **2017**, *124*, 642−650.

DOI: 10.1021/acs.jpcc.7b09643
J. Phys. Chem. C 2018, 122, 2113−2121